Desalination and Water Treatment
www.deswater.com

doi: 10.5004/dwt.2018.22787

123 (2018) 300–308
August

Biosynthesis, characterization and enhanced photocatalytic and antibacterial activity of *Paspalidium flavidum* mediated ZnO nanoparticles

Priyanka[a], Harpreet Kaur[a,*], Anita Thakur[a], Mu. Naushad[b,*]

[a]*Department of Chemistry, Punjabi University, Patiala-147002, Punjab, India, emails: priyag13.garg@gmail.com (Priyanka), preetjudge@yahoo.co.in (H. Kaur), anita3316@gmail.com (A. Thakur)*
[b]*Department of Chemistry, College of Science, Bld#5, King Saud University, Riyadh, Saudi Arabia, email: shad81@rediffmail.com*

Received 12 May 2018; Accepted 10 July 2018

ABSTRACT

Synthesis of nanoparticles using green synthetic route achieving much more importance, because of its simple, clean, nontoxic and eco-friendly approach and it is a better alternate for chemical and physical methods. This work demonstrates the bio-synthetic route for the synthesis of zinc oxide nanoparticles using *Paspalidium flavidum* (weed grass) plant extract. The synthesized nanoparticles were characterized using various analytical techniques. The photocatalytic degradation of amido black 10B dye was also performed using prepared nanoparticles under sunlight luminance. The antibacterial activity against *Bacillus subtilis* and *Pseudomonas aeruginosa* bacteria confirmed that biosynthesized nanoparticles exhibit excellent activity against *B. subtilis*.

Keywords: Paspalidium flavidum; Green synthesis; ZnO; Photocatalytic activity; Antibacterial activity

1. Introduction

Nanotechnology is a process of controlling matter on atomic or molecular scale for constructing functional materials, devices or even systems. The nanoscale has fundamental properties of thermal conductivity, electronic conduction and tensile strength [1,2]. The nanoparticles are unknowingly used for staining drinking glasses and curing certain disease since long, but nowadays, more frequently integrated into various industries, diagnostic techniques, medicines (in drugs, antimicrobial bandages, disinfectant, etc.), cosmetics (sunscreens, talcum powders, etc.), optics, space and in reducing pollution by eliminating the use of toxic materials [3,4]. This technology is already very much entrenched in our life, but still there is space for discovery and integration of nanosystems for the improvement of technologies. Recently, biosynthetic methods which either use biological microorganisms or plant extract for synthesizing metal nanoparticles with specific properties has attracted the attention of modern researchers [5,6]. These metal nanoparticles can be produced from waste plant products (Phytonanotechnolgy) with nontoxicity, biocompatibility and medical applicability, which may fulfil the high demands of biomedical and environmental fields [7–9].

Zinc oxide is a wide band gap semiconductor of the II–VI semiconductor group with excitation energy of 60 meV and broadband gap of 3.37 eV [10]. ZnO NPs are always the centre of attraction due to their wide range of extensive properties, such as bio-sensor [11], gas sensors [12,13], LEDs [14], electrode material in lithium-ion batteries [15] and for the treatment of skin diseases [16].

Dye contaminants from various industries demonstrate a fundamental role to damage the environment [17–21]. One of the most harmful dye, amido black 10B commonly known as naphthol blue black is frequently used in plastic, paint, leather industries and fabrics [22–24]. Due to the persistent, toxic, nonbiodegradable and carcinogenic nature, it can adversely affect the environment [25]. Thus treatment of wastewaters containing dye is extremely essential for the safety of both human and marine ecosystems [26–32]. ZnO NPs are semiconductor-mediated photocatalyst and during photolysis, hydroxyl and superoxide radicals have

* Corresponding author.

been generated and degrade the dye molecules and organic pollutant into nontoxic by-products.

Paspalidium flavidum a weed grass, which is 10–70 cm long and found in culms [33,34]. The secondary metabolites, such as alkaloids, flavonoids, tannins and saponins, are present in *P. flavidum* [35]. These metabolites act as stabilizing agents, so responsible for the reduction in size of ZnO NPs and also the high flavonoids content imparts properties, such as antiinflammatory, analgesic, antioxidative, antifungal, antibacterial and immonustimulant to the weed grass [36–38].

Thus with this perspective, the ZnO NPs were prepared from the weed grass *P. flavidum* and characterized by scanning electron microscopy (SEM), energy dispersive X-ray spectroscopy (EDS), X-ray diffraction (XRD) and Fourier transform infrared spectroscopy (FT-IR) techniques. The photocatalytic degradation of amido black 10B dye was performed using prepared nanoparticles under sunlight luminance. The antibacterial activity was also performed against *Bacillus subtilis* and *Pseudomonas aeruginosa*.

2. Experimental

2.1. Materials

All chemicals utilized in the work were of analytic grade and all solutions were prepared using deionized water. The chemicals, such as zinc nitrate and sodium hydroxide (for NPs preparation), potassium dichromate and mohr's salt (chemical oxygen demand (COD) determination), amido black 10B dye (photocatalytic activity), were procured from MERCK and LOBA (AR) and used without any purification. 100 ppm solution of dye was prepared as a stock solution and it was further diluted with deionized water. *P. flavidum* (weed grass) has been sourced from Punjabi University, Patiala.

2.2. Method

2.2.1. Preparation of plant extract

Wild populations of *P. flavidum* were collected from Botanical garden of Punjabi University, Patiala, Punjab, India. The sample was washed with deionized water to eliminate the dust or impurities and shade dried at room temperature for at least 24 h to remove moisture. The dried leaves were then stored in desiccator for subsequent uses. For the preparation of the fresh extract, 10 g of dried leaves were poured in 100 mL deionized water and then boiled for 30 min until the solution's colour changes from transparent to pale yellow. Then, the extract was cooled, filtered and centrifuged to remove undissolved materials.

2.2.2. Synthesis of ZnO NPs

ZnO NPs were synthesized by green route using *P. flavidum* and zinc nitrate as a precursor. The aqueous solution of NaOH (2 M) with pH = 12 was used to obtain the colloidal solution of nanoparticles. Stoichiometric amount of zinc nitrate, that is, 0.50 mg was dissolved in 100 mL deionized water and stirred with magnetic stirrer. Along with stirring, 8 mL of leaf extract was added dropwise. After 10 min of stirring, drop-wise addition of 6 mL of 2 M aqueous NaOH solution was done. During the addition, colloidal milky coloured solution was obtained. The obtained solution was kept for 2 h so that white colour ZnO NPs were settled down at the bottom of the beaker. The solution was filtered and washed four times with deionized water and then dried in desiccator. The nanoparticles were prepared by varying the concentrations of the plant extract (8, 10, 12 and 14 mL), amount of NaOH (4, 6, 8 and 10 mL), stirring time (10, 15 and 20 min) and different pH (3, 5, 7, 9, 11 and 12).

2.2.3. Characterization techniques

The elemental composition and surface morphology of NPs were examined by SEM attached with EDS using Hitachi SU-8010 SEM instrument. The crystal structure and phase purity of synthesized sample were determined by Rikaguminiflex 600 X-ray diffractometer using Cu-α radiation (λ = 1.54 Å), working at 40 kV, 15 mA with scanning speed of 4.000° min^{-1}. IR spectra were obtained using FTIR spectrophotometer (Perkin-Elmer spectrophotometer – RXI). The optical and photocatalytic properties of ZnO NPs were characterized based on UV absorption spectra using double beam UV-visible spectrophotometer (UV-1800 Shimadzu, Japan). The products obtained after dye degradation were identified using liquid chromatography mass spectrometry (LCMS) technique.

2.2.4. Antibacterial activity

Disc diffusion method was used to study the antibacterial activity of ZnO NPs against *B. subtilis* and *P. aeruginosa* bacteria. Sterilized nutrient agar medium of pH 7.0 containing yeast extract (2.0 g/L), beef extract (1.0 g/L), peptone (5.0 g/L), NACl (5.0 g/L) and agar (15 g/L) was poured in autoclaved petri plates under laminar flow bench. ZnO NPs were sonicated until a uniform colloidal suspension was formed to yield a powder concentration of 2 mg/mL. To assess the toxicity range of nanoparticles against bacteria, volume of 10 μL of ZnO solution was poured in disc. The plates were then incubated at 37°C. The zone of inhibition (ZOI) was measured after 24 h of incubation.

2.2.5. Photocatalytic degradation of dye

The photocatalytic degradation of amido black 10B dye using ZnO NPs was carried out under solar irradiation. In typical procedure, 100 mL dye solution containing fixed amount of NPs was stirred for half an hour on magnetic stirrer and then irradiated under sunlight for three and half hours. 5 mL solution of dye was withdrawn at predetermined time intervals, filtered and centrifuged. With the help of UV-visible spectrophotometer, absorbance of dye solution was measured from which degradation percentage was found by the following formula:

$$\text{Percentage degradation} = \frac{C_0 - C_t}{C_0} \times 100$$

where C_0 is initial concentration of dye and C_t is concentration of dye at time *t*.

To measure the efficiency of photodegradation of amido black 10B, the COD has been taken as another parameter. For COD determination, volumetric analytical method has

been used in which organic compound has been oxidized by strong oxidizing agents, such as $K_2Cr_2O_7$.

$$CH_2O + Cr_2O_7^{2-} + H^+ \rightarrow CO_2 + Cr^{3+} + H_2O$$

For COD determination, 2.0 mL solution of 0.25 N $K_2Cr_2O_7$ and 1.0 mL of deionized water has been taken in titration flask. One to two drops of ferroin indicator has been added and the solution has been shaken for 5 min. This bluish green solution has been titrated against 0.1 N Mohr's salt solution till reddish colour is obtained. The volume of 0.1 N Mohr's salt consumed has been recorded. The volume used is the blank titration reading is '*x*'. The same procedure is repeated with 1.0 mL of dye solution. The volume of Mohr salt solution used in the sample titration reading is '*y*'.

COD determination:

$$\text{COD} = \frac{N \times 1{,}000 \times 8}{\text{Volume of effluent}\left(\frac{\text{mg}}{\text{L}}\right)} \times (x - y)$$

where x = blank titration reading; y = sample titration reading.

The percentage of COD reduction was calculated by using the formula:

$$\text{Percentage COD reduction} = \frac{\text{COD}_0 - \text{COD}_t}{\text{COD}_0} \times 100$$

where COD_0 = initial COD value; COD_t = COD value at time '*t*' after photodegradation.

The data has been applied to pseudo-first-order kinetics model and the equation is given below:

$$\ln\left(\frac{C_0}{C_t}\right) = kt$$

where k is apparent rate constant.

3. Result and discussion

3.1. Characterization of ZnO NPs

The physical properties including shape, size, colour, crystallinity, morphology, etc. play a vital role in characterization of NPs. The synthesized NPs were white in colour and insoluble in water, benzene, chloroform, dimethyl sulphooxide and dimethyl formamide. The size, shape and surface morphology were examined by using the following techniques, such as XRD, EDS, SEM and FT-IR.

3.1.1. X-ray diffraction

X-ray diffraction is an influential analytical technique to analyse the structural features, such as average size, cell spacing, shape and crystal structure of crystalline samples. Fig. 1 displays the XRD spectrum of ZnO NPs and Table 1 depicts XRD parameters. The X-ray diffraction peaks appeared at angles 32.406, 35.070, 36.896, 48.178, 57.244, 63.502, 67.011 and 77.571 corresponds to diffractional planes (100), (002), (101), (102), (110), (103), (112) and (202) (JCPDS card 36–1,451), respectively, approving hexagonal wurtzite structure of synthesized NPs. By taking the full width at half maxima (FWHM) of these peaks, the average size of nanocrystallines has been calculated using Debye–Scherrer formula [39]:

$$D = \frac{k\lambda}{\beta \cos\theta}$$

where λ is the X-ray wavelength of Cu K_α radiation (0.154 nm), k (=0.9) is the shape factor, θ is the Bragg's angle and β is the experimental FWHM of the respective diffraction peak (in units of radians). The average size of NPs has been found to be 22.65 nm.

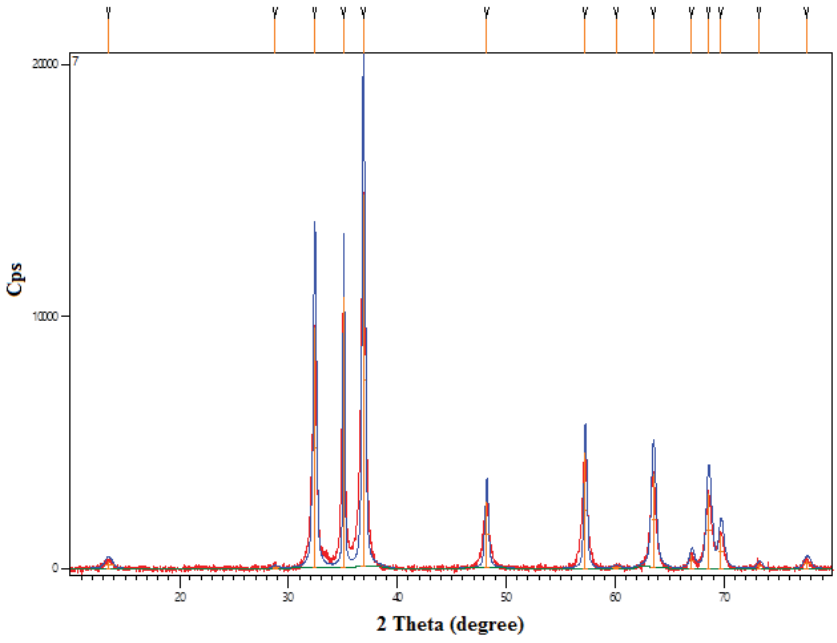

Fig. 1. XRD pattern of synthesized ZnO nanoparticles.

Table 1
XRD parameters for synthesized ZnO NPs

S. No.	2θ (degrees)	*d* (Å)	FWHM (degrees)	Size (nm)
1.	13.481	6.56819	0.818	10.87
2.	28.763	3.10381	0.614	13.37
3.	32.406	2.76279	0.332	24.88
4.	35.070	2.55874	0.153	54.41
5.	36.896	2.43620	0.281	29.75
6.	48.178	1.88881	0.307	28.40
7.	57.244	1.60936	0.281	32.18
8.	60.095	1.53966	0.818	11.22
9.	63.502	1.46502	0.460	20.29
10.	67.011	1.39657	0.460	20.70
11.	68.580	1.36841	0.511	18.79
12.	69.714	1.34890	0.511	18.90
13.	73.222	1.29268	0.511	19.35
14.	77.571	1.23072	0.761	14.22

The Lattice parameters '*a*' = 3.22 Å and '*c*' = 5.16 Å for hexagonal wurtzite system have been calculated by the following equation [40]:

$$\mathrm{Sin}^2\theta = \frac{\lambda^2}{4}\left[\frac{4}{3}\left(h^2 + hk + k^2\right)\frac{1}{a^2} + \frac{l^2}{c^2}\right]$$

3.1.2. SEM and EDS analyses

The morphology and structure of prepared NPs were investigated by using SEM. Morphology and microstructure of ZnO NPs according to SEM analysis (Fig. 2) were floral shape with rough and porous surface. Fig. 3 and Table 2 correspond to the EDS analysis of synthesized NPs with 49.61% zinc, 24.05% oxygen and 26.34% carbon, respectively, which confirmed the presence of plant part (may be flavonoids or cellulose) along with ZnO NPs. EDS results are in good agreement with the XRD results.

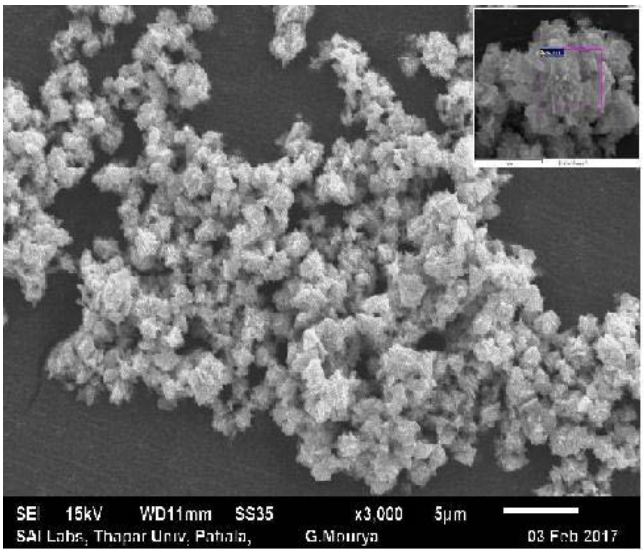

Fig. 2. SEM images of synthesized ZnO nanoparticles.

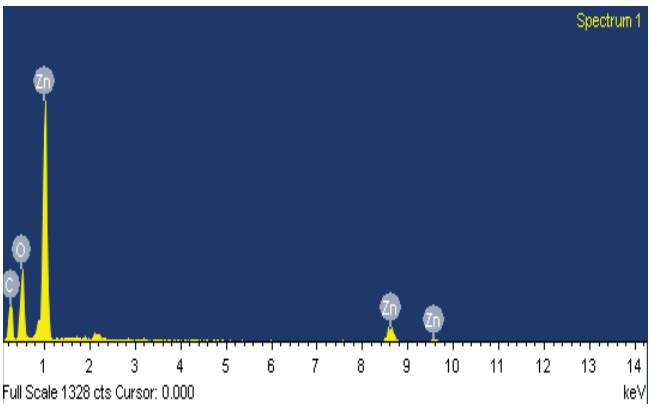

Fig. 3. Energy dispersive spectra of synthesized ZnO NPs.

Table 2
EDS analysis data for synthesized ZnO NPs

Element	Percentage weight	Percentage atomic weight
Zn	49.61	17.03
O	24.05	33.74
C	26.34	49.23

3.1.3. FT-IR analysis

For investigation of the functional group of capping agent associated with synthesized particles, FT-IR spectroscopic studies were performed which are shown in Fig. 4. The IR spectra consist of bands at 544, 910, 3,367.58, 1,649.83, 2,920.75 and 2,104.92 cm^{-1}. The peak appeared at 544 cm^{-1} might be attributed to Zn–O bond, while the band at 910 cm^{-1} may correspond to C–C stretching vibrations. The broad band appearing at 3,367.58 cm^{-1}, that is, at shifted position may be assigned to O–H stretching mode [41–43]. FT-IR spectra showed the presence of peak at 1,649.83 cm^{-1} may be due to O–H bending of absorbed water or carbonyl group. The band present at 2,920.75 cm^{-1} may correspond to asymmetric C–H stretch. The band present at 1,385.53 cm^{-1} may correspond to C–H bending in the plane [44].

3.2. Factors affecting yield of ZnO NPs

A range of factors including amount of extract, volume of NaOH and pH was studied and it was found that these factors affect the yield of NPs.

To study the effect of amount of plant extract on yield of nanoparticles produced, different volume (4, 6, 8, 10, 12 and 14 mL) of extract was added to the solution and it was observed that no product was formed until 8 mL of extract was added. On addition of 8 mL of plant extract, large quantity of product was obtained. Further addition of extract did not affect the yield of NPs.

Various volume of supporting electrolyte, that is, NaOH was used for the synthesis of NPs and it was found that

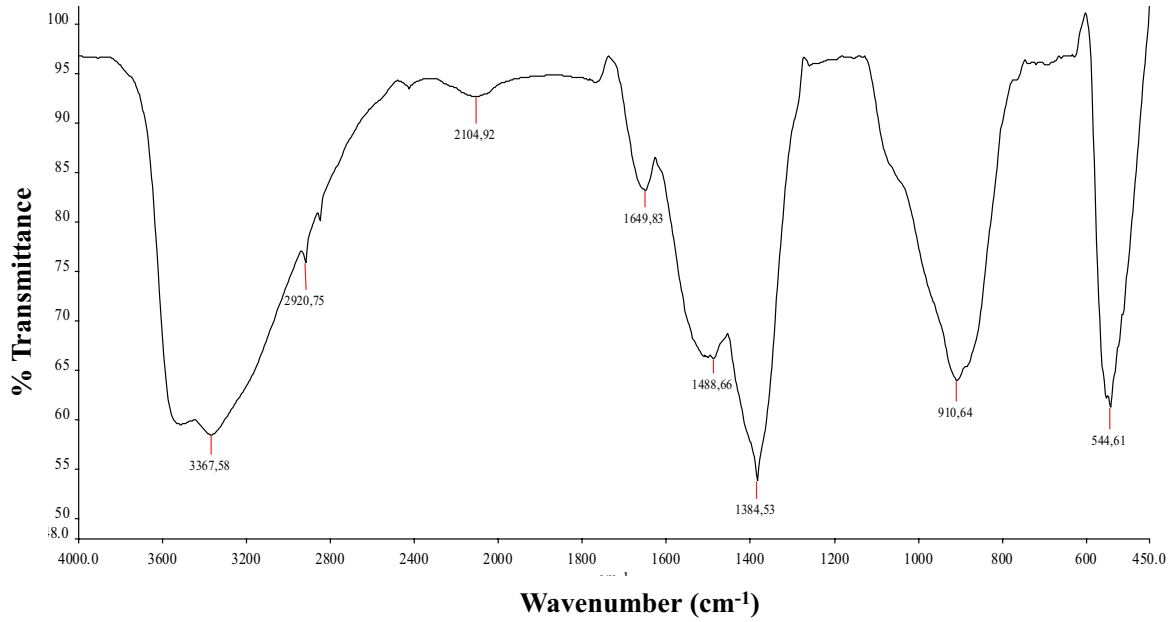

Fig. 4. IR spectrum of synthesized ZnO NPs.

on addition of 2 and 4 mL of 2 M NaOH, no product was formed, but with 6 mL of NaOH, there was formation of product. Further addition of NaOH did not effect on the yield of product.

The pH of solution is also a significant parameter so that the synthesis of NPs was carried out by varying the pH value 3, 5, 7, 9, 11 and 12. It was noticed that between pH 9 to 11, there was the formation of nanoparticles but yield was low, on further increasing pH to 12, yield was increased for fixed concentration of NaOH solution.

3.3. Optical characterization

The optical band gap of synthesized ZnO NPs was measured with the help of UV-visible spectrophotometer in the range of 200–700 nm. The band gap was calculated by the following formula [45]:

$$E_g = \frac{hc}{\lambda}$$

where E_g is optical band gap, c is the speed of light in vacuum, h is Planck's constant and λ is photon's wavelength. The calculated band gap at a wavelength of 365 nm was found to be 3.4 eV (Fig. 5). The reported value in the literature was found to be 3.3 eV, which is less than the present value, confirmed that present synthesized NPs having great optical activity [46].

3.4. Photocatalytic activity

Due to the enhanced photocatalytic activity and formation of nontoxic by-products during photocatalysis, ZnO turned out to be a superior photocatalyst [47]. In photocatalysis, hydroxyl and superoxide-containing radicals were formed, which are responsible for the degradations of dyes and other organic pollutants [48]. The plausible reaction mechanism of photocatalysis as reported in literature is given as follows:

$$\mathrm{ZnO} + \text{Amido black 10B} \rightarrow \mathrm{ZnO}_{(\text{dye adsorbed})}$$

$$\mathrm{ZnO}_{(\text{dye adsorbed})} + \mathrm{hv} \rightarrow \mathrm{ZnO}\left(\mathrm{e}^{-}_{\mathrm{CB}} + \mathrm{h}^{+}_{\mathrm{VB}}\right)_{\text{dye adsorbed}}$$

$$\mathrm{ZnO}\left(\mathrm{h}^{+}_{\mathrm{VB}}\right)_{\text{dye adsorbed}} + \mathrm{H_2O} \rightarrow \mathrm{ZnO}\left(\mathrm{OH}\right)^{\bullet}_{\text{dye adsorbed}} + \mathrm{H}^{+}$$

$$\mathrm{ZnO}\left(\mathrm{e}^{-}_{\mathrm{CB}}\right)_{\text{dye adsorbed}} + \mathrm{O_2} \rightarrow \mathrm{ZnO}\left(\mathrm{O_2}\right)^{\bullet-}_{\text{dye adsorbed}}$$

$$\mathrm{O_2^{\bullet-}} + \mathrm{OH^{\bullet}} + \mathrm{ZnO}_{\text{dye adsorbed}} \rightarrow \text{degradation product} + \mathrm{ZnO}$$

In the work, photodegradation of amido black 10B dye was used to assess the photocatalytic activity of prepared NPs. The effect of different factors, such as the concentration of dye, NPs amount and pH on degradation of dye, was studied and discussed below.

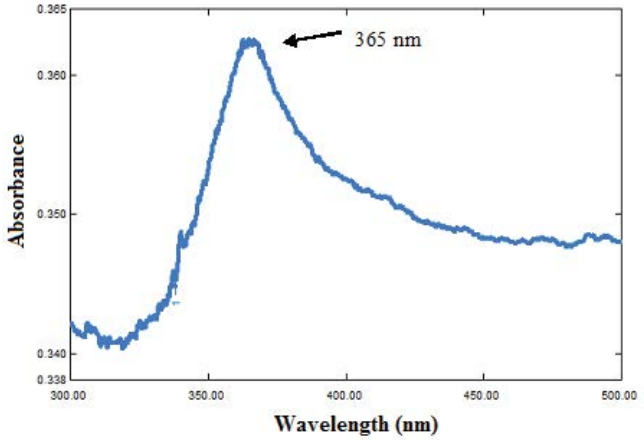

Fig. 5. UV-visible spectra of ZnO NPs.

The effect of initial dye concentration and contact time were investigated by changing the concentration of dye from 30 to 50 mg L^{-1} with time intervals of 30–210 min. The data designate that the percentage removal of dye was decreased with increase in concentration but increased with time of photolysis (Fig. 6). At lower concentration, the available binding sites were occupied by the dye molecules, which resulted in better degradation of dye, but as the concentration increased, the surface active sites on the surface of NPs were decreased, thereby lowering the rate of formation of hydroxyl radicals [49]. The effect of amount of NPs on degradation was also been studied and it is clear from Fig. 7 that the rate of dye degradation increased with increase of amount of NPs due to increase of surface area. But optimum amount of NPs was found to be 0.2 g, because at higher concentration (0.3 g) agglomeration of NPs occurred, resulted in decrease in surface area and causes dye degradation [50]. The effect of pH on degradation process is shown in Fig. 8. ZnO is amphoteric in nature, so at lower pH value zinc oxide forms salt while at higher pH it forms complex $[Zn(OH)_4]^{2-}$. At pH value 6.8, that is, at the actual pH of dye it shows best results in comparison with low and high pH.

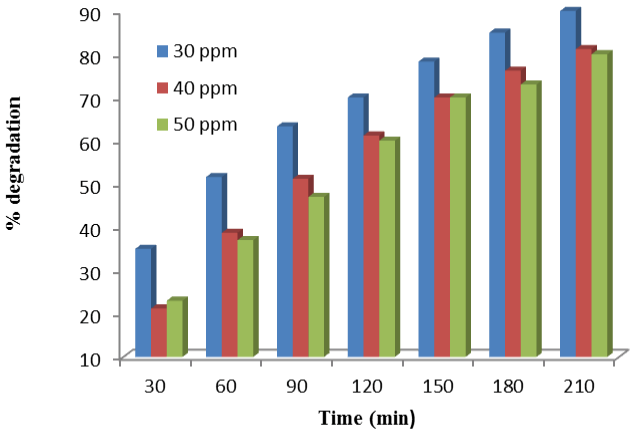

Fig. 6. Effect of contact time and initial dye concentration on percentage degradation of dye.

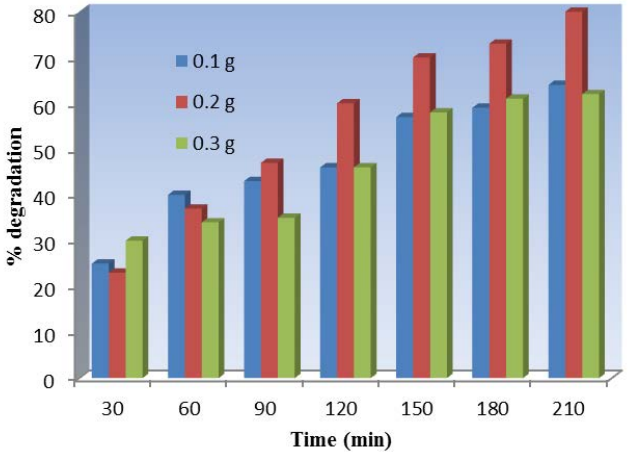

Fig. 7. Effect of amount of ZnO NPs on percentage degradation of amido black 10B dye.

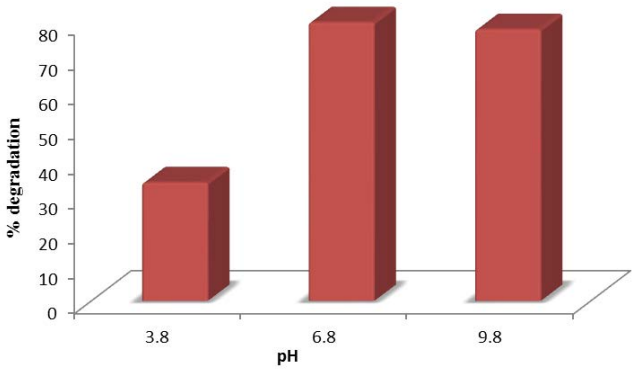

Fig. 8. Effect of pH on percentage degradation of amido black 10B.

COD is the measurement of the amount of organic matter present in a sample and it allows the feasibility of waste in terms of the total amount of oxygen, that is, essential for the oxidation of organic matter to CO_2 and H_2O. The degradation efficiency of ZnO NPs was evaluated through COD analysis for treated and untreated dye solution. It was observed that COD reduction percentage was decreased with increase of amount of NPs and maximum reduction was obtained with 0.2 g of particles (Fig. 9). In case of pH, the percentage reduction was increased with increase of pH, that is, in acidic medium COD reduction was found to be 5.8%, whereas in basic medium it was increased up to 27.2%.

3.4.1. Kinetics of degradation

The data obtained after degradation of dye in the presence of ZnO NPs has been subjected to Langmuir–Hinshelwood equation [51], that is,

$$\ln\left(\frac{C_0}{C_t}\right) = kt$$

For pseudo-first-order kinetic model, a linear plot between $\ln(C_0/C_t)$ versus time is shown in Fig. 10, from which the value of rate constant (k) was calculated, which is 0.007 min^{-1} with good regression coefficient value (R^2 = 0.99).

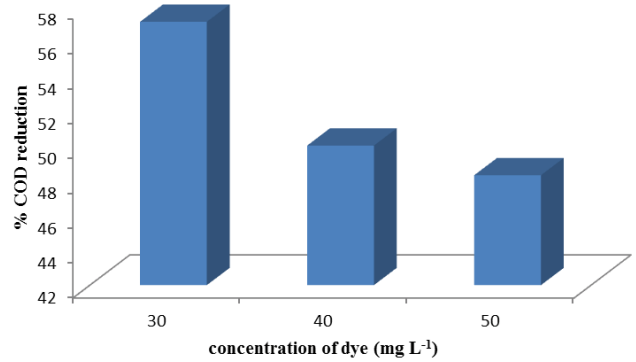

Fig. 9. Concentration of dye versus COD reduction.

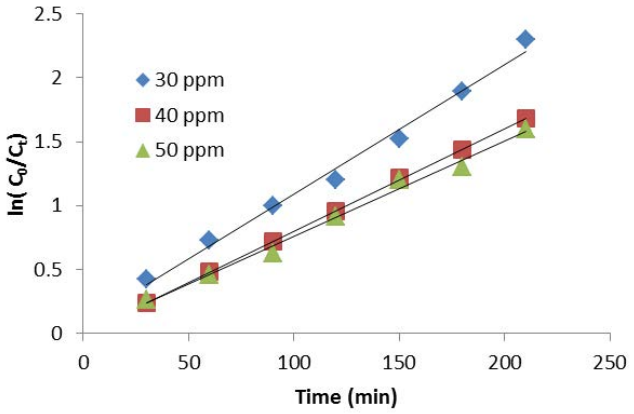

Fig. 10. Pseudo-first-order kinetic plot for degradation of dye at different initial concentration.

3.4.2. LC-MS study

LC-MS spectra of solution were obtained after degradation of amido black 10B dye in the presence of ZnO NPs as catalyst. The spectra consist of peak corresponds to molecular mass 616, 513, 466, 433, 443, 398, 293, 170, 142, 90, 77 and 63. Thus from LCMS peaks it may be concluded that benzene (molar mass 78.11 g/mol) and cyclopentane (molar mass 71.1 g/mol) were the end product on degradation of dye amido black 10B.

3.5. Antibacterial study

Antibacterial study of ZnO was measured against *B. subtilis* (gram positive) and *P. aeruginosa* (gram negative) bacterial strains by measuring the ZOI. It was noted that synthesized NPs have great activity against gram-positive bacteria but is completely inactive against gram-negative bacteria. The ZOI was found to be 28 mm against *B. subtilis* at the concentration of 200 mM. Maximum ZOI is due to the small sized NPs, which penetrate into cell membrane. This penetration may causes disturbance into membrane due to production of reactive oxygen species that kills the bacteria [52]. On comparing the result of antibacterial activity of ZnO nanoparticles with traditional antibiotics, it was observed that ZnO nanoparticles synthesized by biochemical method showed more activity and the results obtained from literature are described in Table 3.

Table 3
Zone of inhibition (mm) against *Bacillus subtilis* by various antibiotics and ZnO NPs

Synthesis method	Zone of inhibition (mm) by antibiotics/ZnO NPs	References
Chemical method	Nitrofurantoin: 22	[53]
	Tetracycline: 24	
	Nalidixic acid: 18	
	Vancomycin: 25	
	Amoxyclan: 16	
	Getamicin: 21	
	Ciprofloxacin: 11	
	Ceftazidime: 17	
	ZnO NPs: 24	[54]
	Erythromycin: 1–3.2	
	Penicillin: 1–2	[55]
	Tetracyclin: 1–4	
	Ampicillin: 1–2	
Sol–gel combustion route	Zno NPs: 25	[56]
Biosynthesis method	ZnO NPs: 28	Present study

4. Conclusion

With the potential use and environmental friendly biosynthesis process, the present investigation demonstrated a simple green synthetic route for the synthesis of ZnO NPs using *P. flavidum* (weed grass) plant extract. The prepared NPs were found to have hexagonal wurtzite structure with size of 22.65 nm and floral shape as confirmed by XRD and SEM analysis. The prepared ZnO NPs were used as photocatalyst for the degradation of amido black 10B under sunlight illumination and also exhibited significant antibacterial activity against *B. subtilis*. The degradation of dye resulted in nontoxic and low-molecular-weight compounds as confirmed by LC-MS study. Thus it was concluded that synthesized nanoparticles had enhanced antibiotic and effective photocatalytic properties.

References

[1] R. Katwal, H. Kaur, G. Sharma, M. Naushad, D. Pathania, Electrochemical synthesized copper oxide nanoparticles for enhanced photochemical and antimicrobial activity, J. Ind. Eng. Chem., 31 (2015) 173–184.
[2] M. Naushad, T. Ahamad, B.M. Al-Maswari, A.A. Alqadami, S.M. Alshehri, Nickel ferrite bearing nitrogen-doped mesoporous carbon as efficient adsorbent for the removal of highly toxic metal ion from aqueous medium, Chem. Eng. J., 330 (2017) 1351–1360.
[3] P. Singh, Y.-J. Kim, D. Zhang, D.-C. Yang, Biological synthesis of nanoparticles from plants and microorganisms, Trends Biotechnol., 34 (2016) 588–599, doi: 10.1016/j.tibtech.2016.02.006.
[4] A.P. Nikalje, Nanotechnology and its applications in medicines, Med. Chem., 5 (2015) 81–89.
[5] X. Li, H. Xu, Z.-S. Chen, G. Chen, Biosynthesis of nanoparticles by microorganisms and their applications, J. Nanomater., 2011 (2011) 16, doi: 10.1155/2011/270974.
[6] S. Ahmed, M. Ahmad, B.L. Swami, S. Ikram, A review on plants extract mediated synthesis of silver nanoparticles for antimicrobial applications: a green expertise, J. Adv. Res., 7 (2016) 17–28.
[7] R.G. Saratale, G.D. Saratale, H.S. Shin, J.M. Jacob, A. Pugazhendhi, M. Bhaisare, G. Kumar, New insights on the green synthesis of metallic nanoparticles using plant and waste biomaterials: current knowledge, their agricultural and environmental applications, Environ. Sci. Pollut. Res. Int., 25 (2018) 10164–10183, doi: 10.1007/s11356-017-9912-6.
[8] Z.U.H. Khan, A. Khan, Y. Chen, N.S. Shah, N. Muhammad, A.U. Khan, K. Tahir, F.U. Khan, B. Murtaza, S.U. Hassan, S.A. Qaisrani, P. Wan, Biomedical application of green synthesized nobel metal nanoparticles, J. Photochem. Photobiol., 173 (2017), 150–164.
[9] L. Gnanasekaran, R. Hemamalini, R. Saravanan, K. Ravichandran, F. Gracia, S. Agarwal, V.K. Gupta, Synthesis and characterization of metal oxides (CeO2, CuO, NiO, Mn3O4, SnO2 and ZnO)

nanoparticles as photo catalysts for degradation of textile dyes, J. Photochem. Photobiol. B., 173 (2017) 43–49.
[10] S. Talam, S.R. Karumuri, N. Gunnam, Synthesis, characterization, and spectroscopic properties of ZnO nanoparticles, ISRN Nanotechnol., 2012 (2012) 6, doi: 10.5402/2012/372505.
[11] E. Topoglidis, A.E.G. Cass, B. O'Regan, J.R. Durrant, Immobilisation and bioelectrochemistry of proteins on nanoporous TiO2 and ZnO films, J. Electroanal. Chem., 517 (2001) 20–27.
[12] X.L. Cheng, H. Zhao, L.H. Huo, S. Gao, J.G. Zhao, ZnO nanoparticulate thin film: preparation, characterization and gas-sensing property, Sens. Actuators B., 102 (2004) 248–252.
[13] S. Saito, M. Miyayama, K. Koumoto, H. Yanagida, Gas sensing characteristics of porous ZnO and Pt/ZnO ceramics, J. Am. Ceram. Soc., 68 (1985) 40–43.
[14] V.V. Multian, A.V. Uklein, A.N. Zaderko, V.O. Kozhanov, O.Y. Boldyrieva, R.P. Linnik, V.V. Lisnyak, V.Y. Gayvoronsky, Synthesis, characterization, luminescent and nonlinear optical responses of nanosized ZnO, Nanoscale Res. Lett., 12 (2017) 164, doi: 10.1186/s11671-017-1934-y.
[15] W. Zhang, L. Du, Z. Chen, J. Hong, L. Yue, ZnO nanocrystals as anode electrodes for lithium-ion batteries, J. Nanomater., 2016 (2016), 7, doi: 10.1155/2016/8056302.
[16] R. Pati, R.K. Mehta, S. Mohanty, A. Padhi, M. Sengupta, B. Vaseeharan, C. Goswami, A. Sonawane, Topical application of zinc oxide nanoparticles reduces bacterial skin infection in mice and exhibits antibacterial activity by inducing oxidative stress response and cell membrane disintegration in macrophages, Nanomed. NBM., 10 (2014) 1195–1208.
[17] D. Pathania, G. Sharma, A. Kumar, M. Naushad, S. Kalia, A. Sharma, Z.A. AlOthman, Combined sorptional–photocatalytic remediation of dyes by polyaniline Zr(IV) selenotungstophosphate nanocomposite, Toxic. Env. Chem., 97 (2015) 526–537.
[18] D. Pathania, D. Gupta, A.H. Al-Muhtaseb, G. Sharma, A. Kumar, M. Naushad, T. Ahamad, S.M. Alshehri, Photocatalytic degradation of highly toxic dyes using chitosan-g poly(acrylamide)/ZnS in presence of solar irradiation, J. Photochem. Photobiol. A: Chem., 329 (2016) 61–68.
[19] A. Thakur, H. Kaur, Response surface optimization of Rhodamine B dye removal using paper industry waste as adsorbent, Int. J. Ind. Chem., 8 (2016) 175–186.
[20] A. Thakur, H. Kaur, Paper industry waste sludge: a low cost adsorbent for the removal of Malachite green dye, Asian J. Chem., 28 (2016) 2139–2145.
[21] R. Kaur, H. Kaur, *Calotropis procera* as effective adsorbent for removal of malachite green dye: a comprehensive study, Desal. Wat. Treat., 78 (2017) 253–262.
[22] A.K. Ojha, V.K. Bulasara, Adsorption characteristics of jackfruit leaf powder for the removal of Amido black 10B dye, Environ. Prog. Sustain. Energy, 34 (2015) 461–470.
[23] A. Mittal, V. Thakur, V. Gajbe, Adsorptive removal of toxic azo dye Amido Black 10B by hen feather, Environ. Sci. Pollut. Res., 20 (2013) 260–269.
[24] R. Kaur, H. Kaur, Electrochemical degradation of Congo Red from aqueous solution: role of graphite anode as electrode material, Port. Electrochem. Acta, 34 (2016) 185–196.
[25] M. Tanzifi, M.T. Yaraki, A.D. Kiadehi, S.H. Hosseini, M. Olazar, A.K. Bhati, S. Agarwal, V.K. Gupta, A.K. Kazemi, Adsorption of Amido Black 10B from aqueous solution using polyaniline/SiO2 nanocomposite: experimental investigation and artificial neural network modeling, J. Colloid Interface Sci., 510 (2018) 246–261.
[26] E. Daneshvar, A. Vazirzadeh, A. Niazi, M. Kousha, M. Naushad, A. Bhatnagar, Desorption of Methylene blue dye from brown macroalga: effects of operating parameters, isotherm study and kinetic modeling, J. Cleaner Prod., 152 (2017) 443–453.
[27] A. Thakur, H. Kaur, Removal of hazardous rhodamine B dye by using chemically activated low cost adsorbent: pine cone charcoal, Int. J. Chem. Phys. Sci., 5 (2016) 17–28.
[28] A.B. Albadarin, M.N. Collins, M. Naushad, S. Shirazian, Activated lignin–chitosan extruded blends for efficient adsorption of methylene blue, Chem. Eng. J., 307 (2017) 264–272.
[29] M. Naushad, Z.A. Alothman, M.R. Awual, S.M. Alfadul, T. Ahamad, Adsorption of rose Bengal dye from aqueous solution by amberlite Ira-938 resin: kinetics, isotherms, and thermodynamic studies, Desal. Wat. Treat., 57 (2016) 13527–13533.
[30] H. Kaur, A. Thakur, Adsorption of Congo red dye from aqueous solution onto ash of *Cassia fistula* seeds: kinetic and thermodynamic studies, Chem. Sci. Rev. Lett., 3 (2014) 159–169.
[31] A.A. Alqadami, M. Naushad, Z.A. Alothman, T. Ahamad, Adsorptive performance of MOF nanocomposite for methylene blue and malachite green dyes: kinetics, isotherm and mechanism, J. Environ. Manage., 223 (2018) 29–36.
[32] M.A.A. Zaini, L.M. Salleh, M. Azizi, C. Yunus, M. Naushad, Potassium hydroxide-treated palm kernel shell sorbents for the efficient removal of methyl violet dye, Desal. Wat. Treat., 84 (2017) 262–270.
[33] J.K. Patra, R.R. Mishra, S.D. Rout, H.N. Thatoi, An assessment of nutrient content of different grass species of Similipal tiger reserve, Orissa, World J. Agric. Sci., 7 (2011) 37–41.
[34] P. Dileep, G.G. Nair, Studies on grass flora associated with paddy field of Wayanad District, Kerala, South India, Ann. Plant Sci., 4 (2015) 1096–1108.
[35] R.H. Babu, N. Savithramma, Screening of secondary metabolites of underutilized species of Cyperaceae, Int. J. Pharm. Sci. Rev. Res., 24 (2014) 182–187.
[36] Alamqeer, M.N.H. Malik, S. Bashir, A.Q. Khan, M.N. Mushtaq, M. Rashid, M. Akram, S. Samreen, Evaluation of diuretic activity of *Paspalidium flavidum* in rats, Bangladesh J. Pharmacol., 8 (2013) 177–180.
[37] P.S. Sandhu, B. Singh, V. Gupta, P. Bansal, D. Kumar, Potential herbs used in ocular diseases, J. Pharm. Sci. Res., 3 (2011) 1127–1140.
[38] Alamgeer, M.N.H. Malik, S. Bashir, I.U. Khan, S. Karim, M.N. Mushtaq, H.U. Khan, M. Rashid, H. Naz, S. Samreen, Cardiotonic and vasoconstriction effects of aqueous methanolic extract of *Paspalidium flavidum* L, Pak. J. Pharm. Sci., 28 (2015) 437–441.
[39] M. Kooti, A.N. Sedeh, Synthesis and characterization of $NiFe_2O_4$ magnetic nanoparticles, J. Mater. Sci. Technol., 29 (2013) 34–38.
[40] B.D. Cullity, Elements of X-ray Diffraction, 2nd ed., Addison-Wesley Publishing Company, Reading, Massachusetts - Menlo Park, California London - Amsterdam - Don Mills, Ontario – Sydney, 1978.
[41] A.A. Alqadami, M. Naushad, Z.A. ALOthman, A.A. Ghfar, Novel metal–organic framework (MOF) based composite material for the sequestration of U (VI) and Th (IV) metal ions from aqueous environment, ACS Appl. Mater. Interfaces, 9 (2017) 36026–36037.
[42] A.B. Albadarin, M. Charara, B.M.A. Tarboush, M.N.M. Ahmad, T.A. Kurniawan, M. Naushad, G.M. Walker, C. Magwandi, Mechanism analysis of tartrazinebiosorption onto masau stones; a low cost by-product from semi-arid regions, J. Mol. Liq., 242 (2017) 478–483.
[43] M. Naushad, Z.A. ALOthman, M.R. Awual, M.M. Alam, G.E. Eldesoky, Adsorption kinetics, isotherms, and thermodynamic studies for the adsorption of Pb2+ and Hg2+ metal ions from aqueous medium using Ti(IV) iodovanadate cation exchanger, Ionics, 21 (2015) 2237–2245.
[44] A. Mittal, M. Naushad, G. Sharma, Z.A. ALothman, S.M. Wabaidur, M. Alam, Fabrication of MWCNTs/ThO_2 nanocomposite and its adsorption behavior for the removal of Pb(II) metal from aqueous medium, Desal. Wat. Treat., 57 (2016) 21863–21869.
[45] S. Kaur, H. Kaur, Photocatalytic studies of electrochemically synthesized polysaccharide-functionalized ZnO nanoparticles, Appl. Nanosci., 8 (2018) 729–738, doi: 10.1007/s13204-018-0815-8.
[46] L.I. Berger, Semiconductor Materials, CRC Press, Boca Raton, FL, 1996.
[47] M. Anbuvannan, M. Ramesh, G. Viruthagiri, N. Shanmugam, N. Kannadasan, Synthesis, characterization and photocatalytic activity of ZnO nanoparticles prepared by biological method, Spectrochem. Acta A., 143 (2015) 304–308.

[48] C.S. Turchi, D.F. Ollis, Photocatalytic degradation of organic water contaminants: mechanism involving hydroxyl radical attack, J. Catalysis, 122 (1990) 178–192.
[49] S. Sunitha, A.N. Rao, Antibacterial and photocatalytic activity of ZnO nanoparticles synthesized by sol-gel method, J. Chem. Pharm. Res., 7 (2015) 1446–1451.
[50] M. Aliabadi, T. Sagharigar, Photocatalytical removal of Rhodamine-B from aqueous solutions using TiO_2 nanocatalyst, J. Appl. Environ. Biol. Sci., 1 (2011) 620–626.
[51] A. Eyasu, O.P. Yadav, R.K. Bachheti, Photocatalytic degradation of methyl orange dye using Cr-doped ZnS nanoparticles under visible radiation, Int. J. Chem. Tech. Res., 5 (2013) 1452–1461.
[52] M.J. Divya, C. Sowmia, K. Joona, K.P. Dhanya, Synthesis of zinc oxide nanoparticles from *Hibiscus rosa-sinensis* leaf extract and investigation of antibacterial activity, Res. J. Pharm. Biol. Chem. Sci., 4 (2013) 1137–1142.
[53] H. Meruvu, M. Vangalapati, S.C. Chippada, S.R. Bammidi, Synthesis and charcaterzation of zinc oxide nanoparticles and its antimicrobial activity against *Bacillus subtilis* and *Escherichia coli*, Rasyan J. Chem., 4 (2011) 217–222.
[54] K. Renugadevi, P. Raji, M. Bavanilatha, In-vitro evaluation of antibacterial activity and cytotoxicity effect of chemically synthesized ZnO nanoparticles, Int. J. Pharm. Sci. Res., 3 (2012) 2639–2643.
[55] K.R. Chandrika, P.K. Mayi, R.V.S.S.N.R. Kumar, Role of ZnO nanoparticles in enhancing the antibacterial activity of antibiotics, Asian J. Pharm. Clin. Res., 5 (2012) 97–99.
[56] A. Azam, A.S. Ahmed, M. Oves, M.S. Khan, S.S. Habib, A. Merric, Antimicrobial activity of metal oxide nanoparticles against gram-positive and gram-negative bacteria: a comparative study, Int. J. Nanomed., 7 (2012) 6003–6009.